PERGAMON

Journal of Structural Geology 25 (2003) 209–221

JOURNAL OF STRUCTURAL GEOLOGY

www.elsevier.com/locate/jsg

Flow patterns around rigid inclusions in a multiple inclusion system undergoing bulk simple shear deformation

Susanta Kumar Samanta[a], Nibir Mandal[a], Chandan Chakraborty[b,*]

[a]Department of Geological Sciences, Jadavpur University, Kolkata 700032, India
[b]Geological Studies Unit, Indian Statistical Institute, 203 B.T. Road, Kolkata 700035, India

Received 8 May 2001; received in revised form 3 February 2002; accepted 10 February 2002

Abstract

During deformation of an inclusion-matrix system, the velocity fields around individual inclusions mutually interfere with one another. Such interacting inclusions rotate at slower rates than non-interacting, single inclusions. This paper presents a theoretical model that describes the flow pattern of matrix (viscous) material around interacting rigid inclusions of spherical shape in bulk simple shear deformation. Numerical simulations based on the velocity functions reveal that the volume concentration of inclusions is a crucial parameter controlling the flow pattern around rotating inclusions under interacting conditions. At low volume concentrations ($\rho_v < 0.01$, where $\rho_v = (a/b)^3$, $2a$: inclusion diameter and $2b$: mean inter-inclusion distance) the flow is characterized by an eye-shaped separatrix, which, with increase in volume concentration ($\rho_v > 0.1$), transforms into a pattern with a bow-tie shaped separatrix. At a large volume concentration ($\rho_v = 0.4$) the separatrix assumes the geometry of a super-ellipse. We also present numerical models that illustrate the influence of volume concentration on the (1) nature of strain distribution, (2) distortion patterns of passive foliations ,and (3) mantle structures around inclusions in an interacting state. Based on this theory, it is shown that the rotational retardation of the inclusions slightly enhances the bulk viscosity of the inclusion-matrix system.

Keywords: Interacting inclusions; Rotation; Velocity functions; Bulk viscosity

1. Introduction

The studies on the deformation behavior of inclusion-matrix rock systems deal with three principal aspects: (1) rigid rotation and deformation of individual inclusions, (2) flow-field around inclusions, and (3) bulk viscosity of the system. It has been revealed that the shape and orientation of the inclusion controls its rotation, in addition to the bulk vorticity (Gay, 1968; Reed and Tryggvason, 1974; Ghosh and Ramberg, 1976; Ferguson, 1979; Freeman, 1985; Fernandez, 1987; Passchier, 1987; Masuda et al., 1995; Jezek et al., 1996; Mandal et al., 2001). There is also a radically different proposition which states that inclusions in certain circumstances may not rotate even when the bulk deformation is non-coaxial (Bell, 1985; Johnson, 1993; Stewart, 1997; Hickey and Bell, 1999; Stallard and Hickey, 2001). As far as the flow field around rigid inclusions is concerned, both theory and experiments show that the deformation of matrix in the neighborhood of individual inclusions is always heterogeneous (Gay, 1968; Ghosh, 1975; Masuda and Ando, 1988; ten Brink and Passchier, 1995; Masuda and Mizuno, 1996; Jezek et al., 1999; Mandal et al., 2001). All these studies, however, consider a single inclusion floating in an infinitely extended, continuous medium and are thus applicable to rocks with very low volume concentrations of inclusions. If inclusions are present in a rock in higher proportions, they are likely to interact with one another affecting the rotation of individual inclusions as well as the surrounding matrix flow, as revealed in analog model experiments (Ildefonse et al., 1992, 1993). Experimental studies also demonstrate that in inclusion-matrix systems interaction may set in due to tiling of the inclusions during progressive shear, even when the volume concentration is low, and the finite rotation of inclusions deviates from that predicted by Jeffery's theory on single inclusion systems (Tikoff and Teyssier, 1994; Arbaret et al., 1996). The mechanical interaction of inclusions also modifies the bulk viscosity of inclusion-matrix systems (Happel, 1957), in addition to other factors such as geometrical and rheological properties of the phase components (Treagus, 2002, and references therein).

The purpose of this paper is to investigate the effects of mutual interaction of *equant* inclusions in a multiple

* Corresponding author. Fax: +91-33-577-6680.
E-mail address: chandan@isical.ac.in (C. Chakraborty).

0191-8141/02/$ - see front matter
PII: S0191-8141(02)00032-9

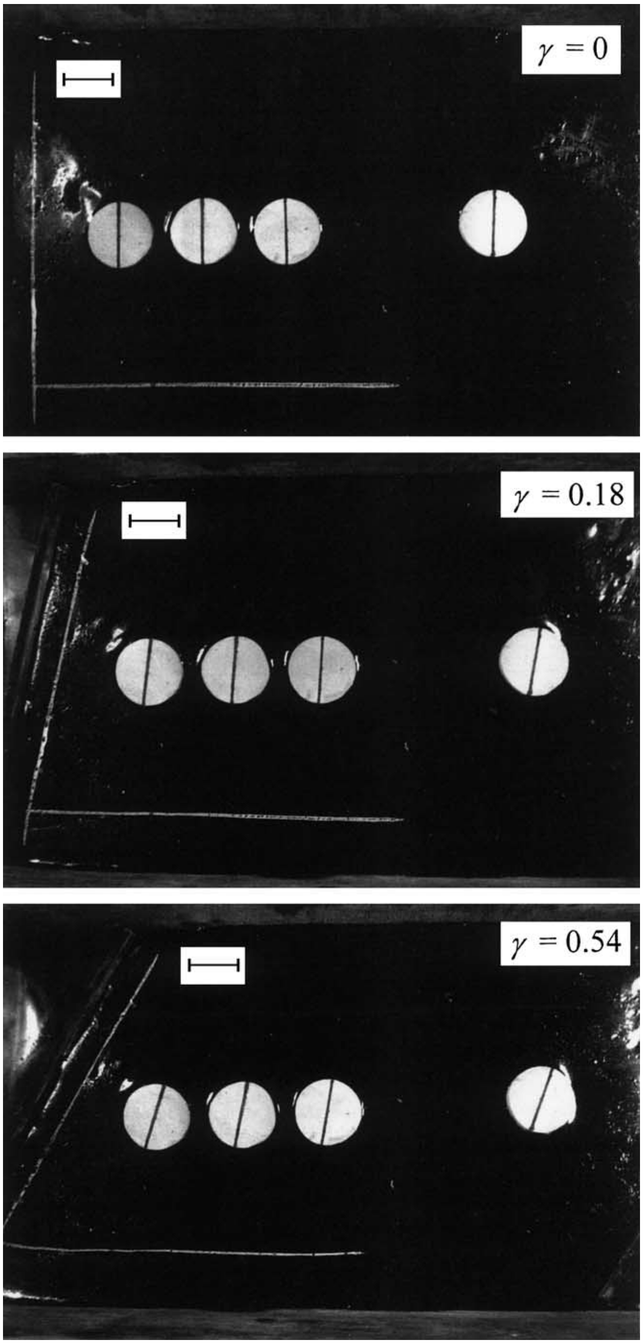

Fig. 1. Successive stages of simple shear (dextral) deformation of model (plan view) containing equant inclusions in a slab of pitch (viscous). Note that closely spaced inclusions in the row have rotated smaller than the inclusion located at a large spacing. The ratio of inclusion diameter to inter-inclusion distance (a/b) was 0.79. Scale bar = 2 cm.

inclusion system on the rotation of, and flow field around, individual inclusions, and the bulk viscosity of the inclusion-matrix system. Simple experiments were performed to study how the presence of inclusions in the neighborhood could retard the rotation of an *equant* inclusion. The paper also presents a theoretical model that derives the rotation rate of rigid inclusions and the velocity functions for the matrix flow in a multiple inclusion system, under simple shear taking into account the effects of interactions of surrounding inclusions. The derived equations are used to run numerical experiments to investigate the influence of mean distance or volume concentration of inclusions on the flow pattern, strain shadow, foliation drag and mantle structure around rigid inclusions. Finally, the paper explores the effects of rotational retardation of rigid inclusions on the bulk viscosity of inclusion-matrix systems.

2. Rotation of interacting inclusions: experimental observations

We performed a set of experiments on viscous models in simple shear to study the rotational behavior of rigid inclusions disposed with spacing allowing mutual interference of the velocity fields around them. The model consisted of three circular cylindrical (wooden) inclusions floating in a viscous (pitch) slab. The viscosity of pitch was about 5×10^5 Pa s at room temperature (30 °C). The inclusions were placed in a row along the central shear plane with their axes along the direction of no-strain to avoid an overall rotation of the inclusion row. The inter-inclusion distance in the row was set between 1.15 and 1.30 (values normalized to inclusion diameter) to obtain a discernible effect of mutual interaction. In order to compare the rotational behavior of the inclusions in an interacting state with that under non-interacting conditions, one inclusion was placed in the same row, but at a large distance from the three interacting inclusions. The experiments were run in simple shear (1.5×10^{-3}/s) at room temperature. During deformation the model base was lubricated with liquid soap to minimize the basal friction in order to obtain largely homogeneous simple shear in the model. Marker lines were drawn parallel and perpendicular to the shear direction to find the finite bulk shear at any stage of deformation in the model. Experiments with specific configurations of the inclusions were repeated under the same conditions to test their reproducibility.

In the experimental runs, the closely spaced inclusions always rotated slower than that located away from them. Among the three closely spaced inclusions, the central one rotated at the slowest rate (Fig. 1) due to mechanical coupling exerted by the rotating inclusions on its either side. We measured the amount of finite rotation of the interacting inclusions at different stages of progressive shear, and compared it with that of the far-field one and predicted from the theory discussed in the following section (Fig. 2). The results clearly indicate that, at any stage of deformation the finite rotation of each inclusion in the row is smaller than the far-field one. Experimental runs with different inter-inclusion distances again reveal that the difference between the rotation rates of closely spaced inclusions and the far-field one is larger for smaller inter-inclusion distance. These simple experiments demonstrate that there may be a discernible retardation in the rotational motion of rigid

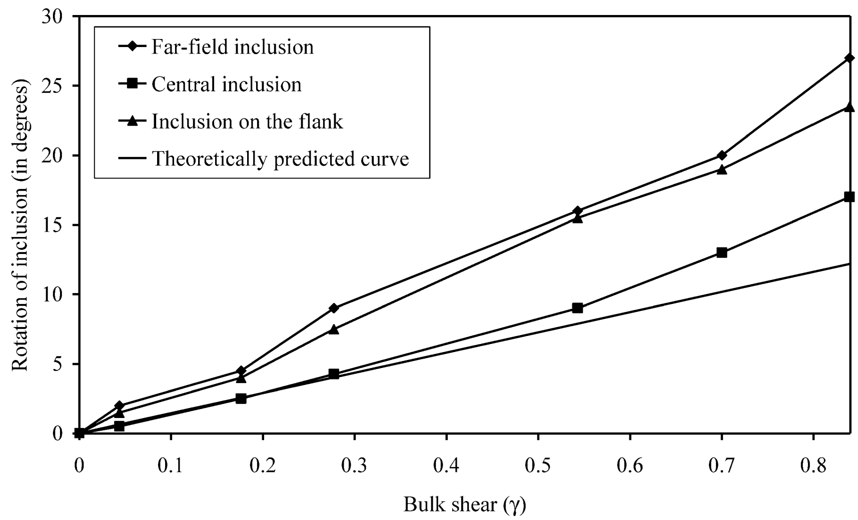

Fig. 2. Plots of finite rotation of inclusions versus bulk shear, as obtained from the test model shown in Fig. 1. Note that: (i) the rotations of inclusions occurring in the row are less than that of the isolated (far-field) one and (ii) the rotation of the central inclusion with the bulk shear is closer to that obtained from the present theoretical model.

inclusions due to mechanical interaction, even when the inclusions are equant in shape. The following section presents a theoretical model describing the flow field around such interacting spherical inclusions in simple shear.

3. Theoretical considerations

3.1. The model

The physical model under consideration consists of uniformly distributed rigid, spherical inclusions of radius a within a Newtonian viscous matrix (Fig. 3a). We assume a non-slip condition at the matrix-inclusion interfaces. The model is subjected to simple shear at a rate $\dot{\gamma}$. We set a Cartesian reference frame (xyz) with the x axis parallel to the shear direction and y axis normal to the shear plane (Fig. 3b). The bulk shear flow ($\dot{\gamma}$), for the sake of mathematical derivation, is resolved into distortion (e_{xy}) and rotation (ζ) parts, where $e_{xy} = \dot{\gamma}/2$and $\zeta = \dot{\gamma}/2$. For a homogeneous shear flow, i.e. in the absence of inclusions, the velocity components (u, v, w) along x, y and z directions for the distortion and rotation parts are represented, respectively, as:

$$u^*_{\mathrm{D}} = \frac{\dot{\gamma}}{2}y; \qquad v^*_{\mathrm{D}} = \frac{\dot{\gamma}}{2}x; \qquad w^*_{\mathrm{D}} = 0 \tag{1a}$$

$$u^*_{\mathrm{R}} = \frac{\dot{\gamma}}{2}y; \qquad v^*_{\mathrm{R}} = -\frac{\dot{\gamma}}{2}x; \qquad w^*_{\mathrm{R}} = 0 \tag{1b}$$

The subscripts D and R stand for distortion and rotation, respectively. The flow perturbations due to the presence of inclusions are determined separately for the distortion (e_{xy}) and rotation (ζ) components of the bulk shear flow, which are added to that of the homogeneous shear flow (Eqs. (1a) and (1b)) to obtain the flow field around an individual inclusion. Appendix A provides the details of the derivations, and an outline is given below.

Considering the distortion part (e_{xy}) of the bulk shear, Happel (1957) derived the expressions of the velocity components of the flow perturbation in terms of spherical co-ordinates (Fig. 3c; Eq. (A2) in Appendix A). As our numerical simulations are developed in two dimensions on a section at right angle to the direction of no bulk strain, we consider the velocity components in terms of Cartesian co-ordinates on the xy-plane (i.e. $z = 0$) as:

$$u_{\mathrm{D}} = \dot{\gamma}\left[f_1(r) - f_2(r)\left(2 - \frac{r^2}{x^2}\right)\right]\frac{x^2 y}{r^3}$$

$$v_{\mathrm{D}} = \dot{\gamma}\left[f_1(r)\left(1 - \frac{x^2}{r^2}\right) + f_2(r)\left(2\frac{x^2}{r^2} - 1\right)\right]\frac{x}{r} \tag{2}$$

where

$$f_1(r) = \left(6r^3 A + 2rB + \frac{6}{r^2}C - \frac{3D}{r^4}\right)$$

and

$$f_2(r) = \left(5r^3 A + rB + \frac{D}{r^4}\right)$$

.A, B, C and D are constants, which are dependent on the ratio of inclusion diameter and inter-inclusion distance (a/b) (see Eq. (A3)).

In order to estimate the flow perturbation for the rotational part (ζ) of the bulk shear flow, we need to consider the rotational behavior of individual inclusions in an interacting state. Experiments reveal that interacting spherical inclusions rotate at slower rates compared with non-interacting ones rotating at rates close to $\dot{\gamma}/2$ (Fig. 2). It can be shown (Eq. (A9) in Appendix A) that the instantaneous

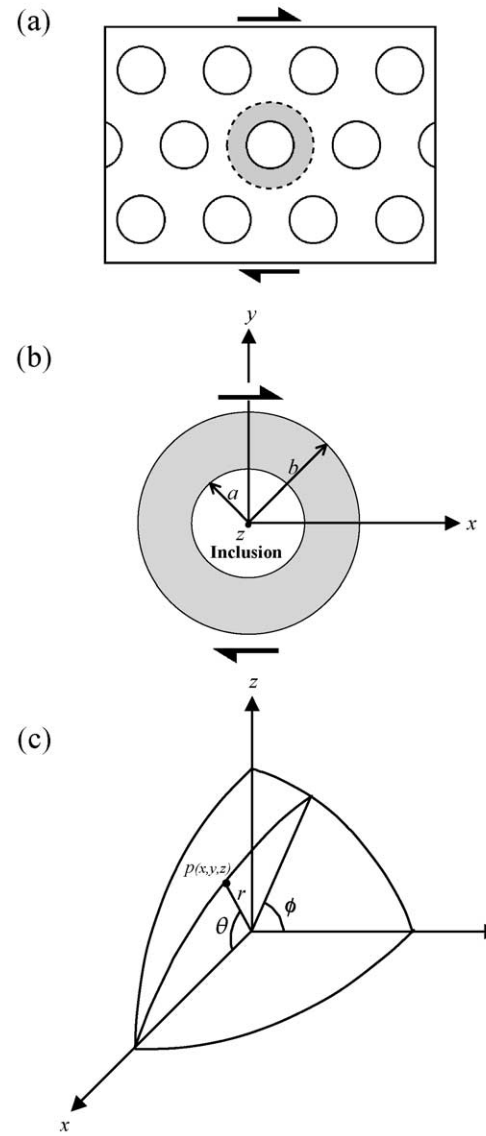

Fig. 3. (a) Model under theoretical consideration. The circles represent the inclusions floating in a matrix. The circle with a shell of matrix (shaded) in its surrounding represents the inclusion around which the flow is modeled taking into account the effects of the neighboring inclusions. (b) Enlarged view of the inclusion shown in (a) showing the choice of Cartesian coordinate reference frame (*xyz*) with origin at the center of the inclusion and *x* axis parallel to the shear direction, and *y* axis normal to the shear plane. A shell (shaded) of radius *b* is considered around the inclusion, on the surface of which the boundary conditions for mechanical interaction with its neighboring inclusions are imposed (see text for details). (c) Relation between the Cartesian frame *xyz* and spherical coordinate system under consideration.

rotation rate of the rigid spherical inclusion in an interacting state is:

$$\omega' = (1 - \alpha^3)\frac{\dot{\gamma}}{2} \tag{3}$$

α is the ratio of inclusion diameter ($2a$) and inter-inclusion distance ($2b$). Eq. (3) shows that the rotation rate of spherical inclusions (ω') increases with inter-inclusion distance (Fig. 4), and assumes a value of $\dot{\gamma}/2$, when b tends to infinity or α tends to be zero, i.e. when rigid inclusions occur in a very low volume concentration to be in a non-interacting state, as obtained from the hydrodynamic theory (Jeffery, 1922). On the other hand, when $b = a$, ω' becomes zero, implying that interacting inclusions cannot rotate independently if they are in contact with one another. It has been inferred from field observations (Bell, 1985) that under certain circumstances porphyroblasts rotate little in non-coaxial deformation, and the rotational component of the bulk deformation has been partitioned in the matrix. Our theoretical analysis suggests that such non-rotational behavior of the porphyroblasts might have resulted from mutual mechanical coupling due to their large volume concentration.

From Eq. (A10) in Appendix A, the flow perturbation in the matrix in response to the rotational part of the bulk shear flow can be expressed as:

$$u_R = -\frac{\dot{\gamma}}{2}\frac{a^6}{b^3 r^3}y$$

$$v_R = \frac{\dot{\gamma}}{2}\frac{a^6}{b^3 r^3}x \tag{4}$$

By adding the velocity components in Eqs. (1a), (1b), (2) and (4), we obtain the flow field around a spherical inclusion on the *xy*-plane of the Cartesian coordinate system as:

$$u = \left[\left(1 - \frac{1}{2}\frac{a^6}{b^3 r^3}\right)y + \left\{f_1(r) - f_2(r)\left(2 - \frac{r^2}{x^2}\right)\right\}\frac{x^2 y}{r^3}\right]\dot{\gamma}$$

$$v = \left[\left(\frac{1}{2}\frac{a^6}{b^3 r^3}\right)x + \left\{f_1(r)\left(1 - \frac{x^2}{r^2}\right) + f_2(r)\left(2\frac{x^2}{r^2} - 1\right)\right\}\frac{x}{r}\right]\dot{\gamma} \tag{5}$$

Eq. (5) represents the velocity field around an individual spherical rigid inclusion surrounded by identical inclusions in an interacting state (Fig. 3a), which is valid in the regime $r < b$ (Fig. 3b). This equation can thus be used to study the flow pattern around individual mechanically interacting inclusions within a multiple inclusion system under simple shear. In this analysis we will use a parameter ρ_v, where $\rho_v = (a/b)^3$, as a measure of volume concentration of inclusions.

3.2. Flow patterns around interacting inclusions

The flow patterns around spherical rigid inclusions are principally of two types: one with eye-shaped separatrix and the other with bow-tie shaped separatrix. It has been shown that the type of flow depends on the matrix rheology (Passchier, 1994; Pennacchioni et al., 2000) and the nature of bulk deformation (Mandal et al., 2001). Numerical simulations, based on the velocity functions in Eq. (5) indicate that the flow pattern depends also on the volume concentration parameter of inclusions ρ_v. At $\rho_v < 0.01$ the flow pattern is characterized by an eye-shaped separatrix with a

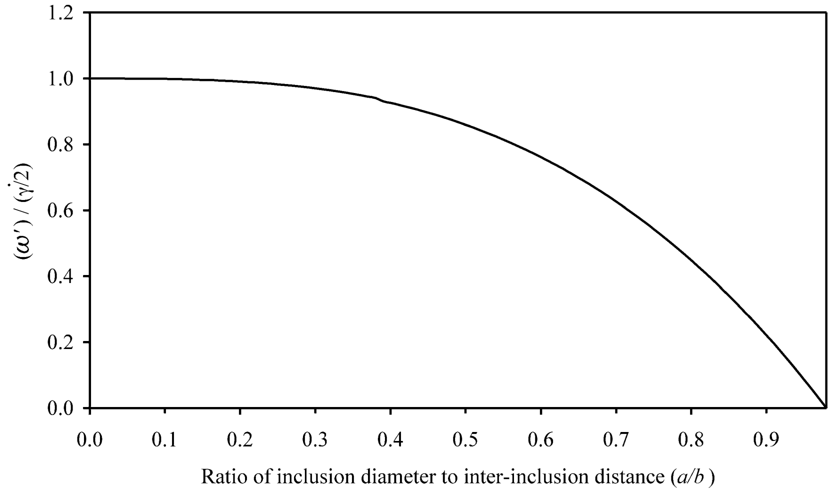

Fig. 4. Non-linear variation of rotation rate (ω') of inclusions with inter-inclusion distance as obtained from theoretical calculations. Note that for large inter-inclusion distances (e.g. $a/b < 0.1$) the rotation rate of inclusion is close to $\dot{\gamma}/2$.

finite dimension only across the shear plane (Fig. 5a; cf. Masuda and Ando, 1988; Mandal et al., 2001), which is similar to that around a non-interacting inclusion. With increase in ρ_v, two stagnation points appear on either side of the inclusion, defining finite dimensions of the separatrix (Fig. 5b). At $\rho_v = 0.1$ the flow assumes a typical pattern with a bow-tie shaped separatrix (Fig. 5c; cf. Passchier, 1994). The separatrix is nearly elliptical in shape with its long dimension lying along the shear direction. With further increase in volume concentration the stagnation points defining the long dimension of the separatrix shift towards the surface of the rigid inclusion reducing the size of the separatrix (Fig. 5d). The shape of the separatrix bounding the close particle paths also varies with increasing volume concentration of inclusions. At a low volume concentration the shape is defined by an ellipse, which tends to assume the geometry of a super-ellipse (Lisle, 1988) with increase in volume concentration (Fig. 5a and d).

4. Geological implications

4.1. Strain distributions

Based on the above theory, numerical model experiments were run to investigate the influence of volume concentration of rigid inclusions on the nature of strain distribution in the matrix around an inclusion. The initial models had small circular markers in a Cartesian grid. The model was deformed by incremental shear strain according to the velocity functions in Eq. (5), following the same procedures described in an earlier publication (Mandal et al., 2001). The shapes and orientations of the deformed markers reveal the nature of strain heterogeneity around a rigid inclusion in an interacting state. When the volume concentration of rigid inclusions is low ($\rho_v < 0.01$), the strain distribution (Fig. 6a) is similar to that observed around a non-interacting, single inclusion in numerical as well as physical model experiments (Masuda and Ando, 1988; Ildefonse et al., 1992; Mandal et al., 2001). With increase in ρ_v, there is an overall increase in finite strain around an inclusion under the same finite bulk shear. At a large value of ρ_v ($= 0.4$) models show a strongly heterogeneous strain distribution, forming curved zones of large finite strain on either side of the rigid inclusion (Fig. 6d). In addition, the *XY* planes of finite strain ellipses away from the inclusion verge antithetically with respect to the shear direction (Fig. 6d).

4.2. Distortion patterns of passive foliations

Previous studies reveal that the initial orientation of the foliation and the ratio of pure shear and simple shear rates control the distortion pattern of the foliation around an inclusion (Ghosh, 1975; Masuda and Ando, 1988; Mandal et al., 2001). Our numerical models indicate that the volume concentration of rigid inclusions is an additional factor that could control the distortion pattern to a large extent. At low volume concentrations ($\rho_v < 0.01$) the distortion pattern is characterized by inwardly convex curvatures of the passive foliation (Fig. 7a), as observed in earlier numerical and physical model experiments (Ghosh, 1975; Masuda and Ando, 1988; Mandal et al., 2001). With increase in ρ_v there is an overall back rotation of the foliations with respect to the bulk shear direction (Fig. 7b and c). At large volume concentrations tight folds, verging synthetically to the shear sense, develop near the surface of the rigid inclusion (Fig. 7d). Secondly, the foliations show a large-scale S-like distortion (Fig. 7d).

It can be noted that the external foliations may be entrapped by growing porphyroblasts, giving rise to diverse, complex types of inclusion trail structures reported from many metamorphic terrains (e.g. Hickey and Bell, 1999). Earlier theoretical and numerical studies indicate that the

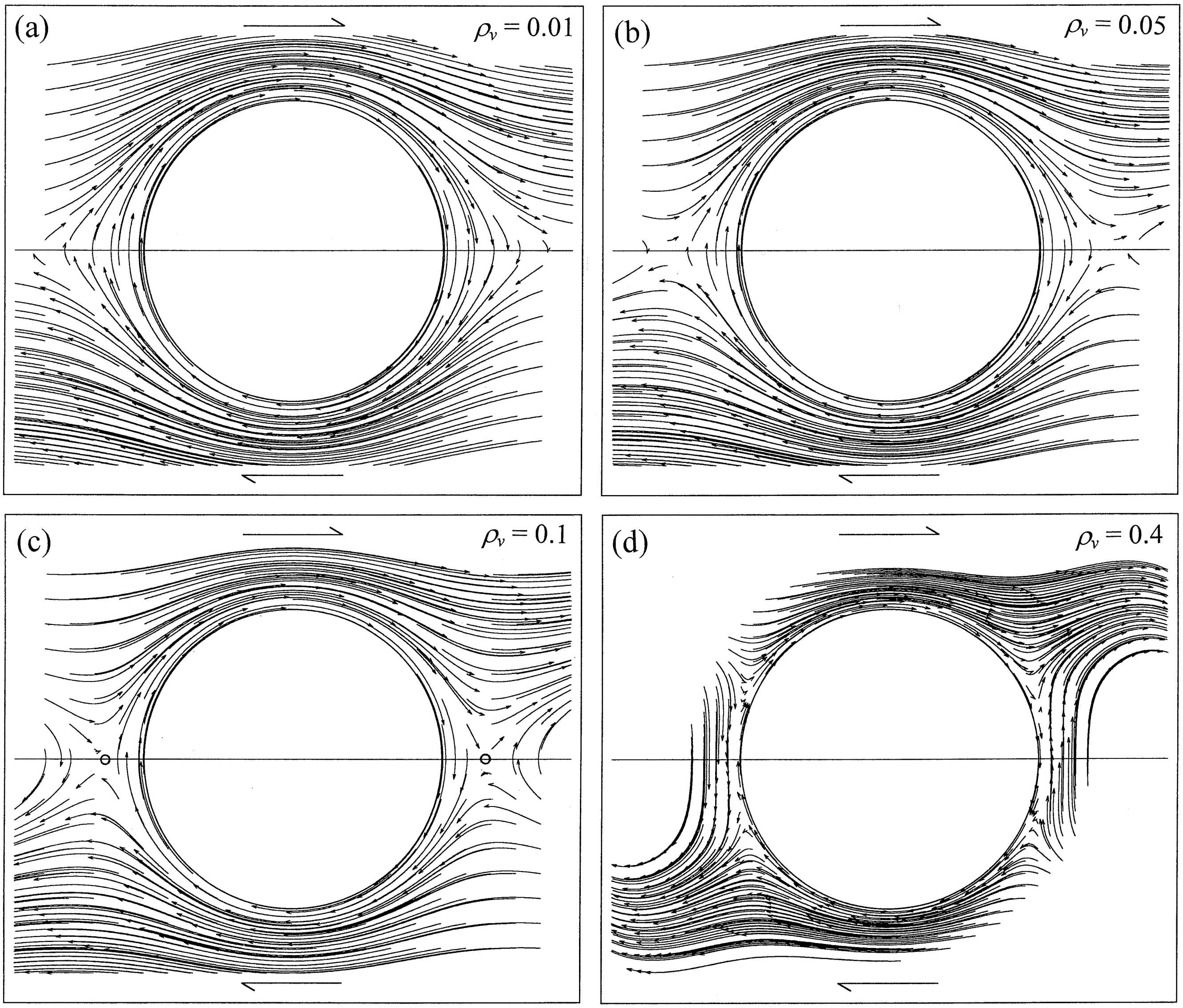

Fig. 5. Contrasting flow patterns around inclusions with increasing values of ρ_v, (where $\rho_v = a^3/b^3$, $2a$: inclusion diameter and $2b$: mean inter-inclusion distance). (a) Flow pattern with eye-shaped separatrix, (b) flow pattern with two stagnation points (o) lying on the central shear plane, on either side of the inclusion, (c) pattern with typical bow-tie shaped separatrix (cf. Passchier 1994), and (d) pattern with the separatrix approximating the geometry of a super-ellipse.

initial orientation of foliation, the shape and orientation of inequant porphyroblasts and the bulk vorticity of deformation or the geometry of overprinting crenulations are the principal factors governing the inclusion trail structure (Samanta et al., 2002, and references therein). The present study suggests that the volume concentration of porphyroblasts is an additional factor determining the distortion pattern of the external foliation and thereby the inclusion trail patterns within the growing porphyroblasts.

4.3. Mantle structures around porphyroclasts

Several physical factors, such as clast-size reduction rate, nature of bulk deformation, clast-shape etc., have been recognized to control the development of different types of mantle structures around porphyroclasts (Passchier and Simpson, 1986; Passchier, 1994; Bjornerud and Zhang, 1995; Masuda and Mizuno, 1996; Mandal et al., 2000b). In this section we investigate the development of mantle structures in multiple porphyroclast systems. A set of experiments was conducted under simple shear by varying the volume concentration of porphyroclasts at a constant clast-size reduction rate. When the volume concentration is low ($\rho_v = 0.01$), the mantle structures develop with incipient δ-type tails (Passchier and Simpson, 1986), which with progressive increase in bulk shear turns into a typical δ, and the mantle finally becomes composite, showing $\delta-\phi$ tails (Fig. 8a). With increase in volume concentration the

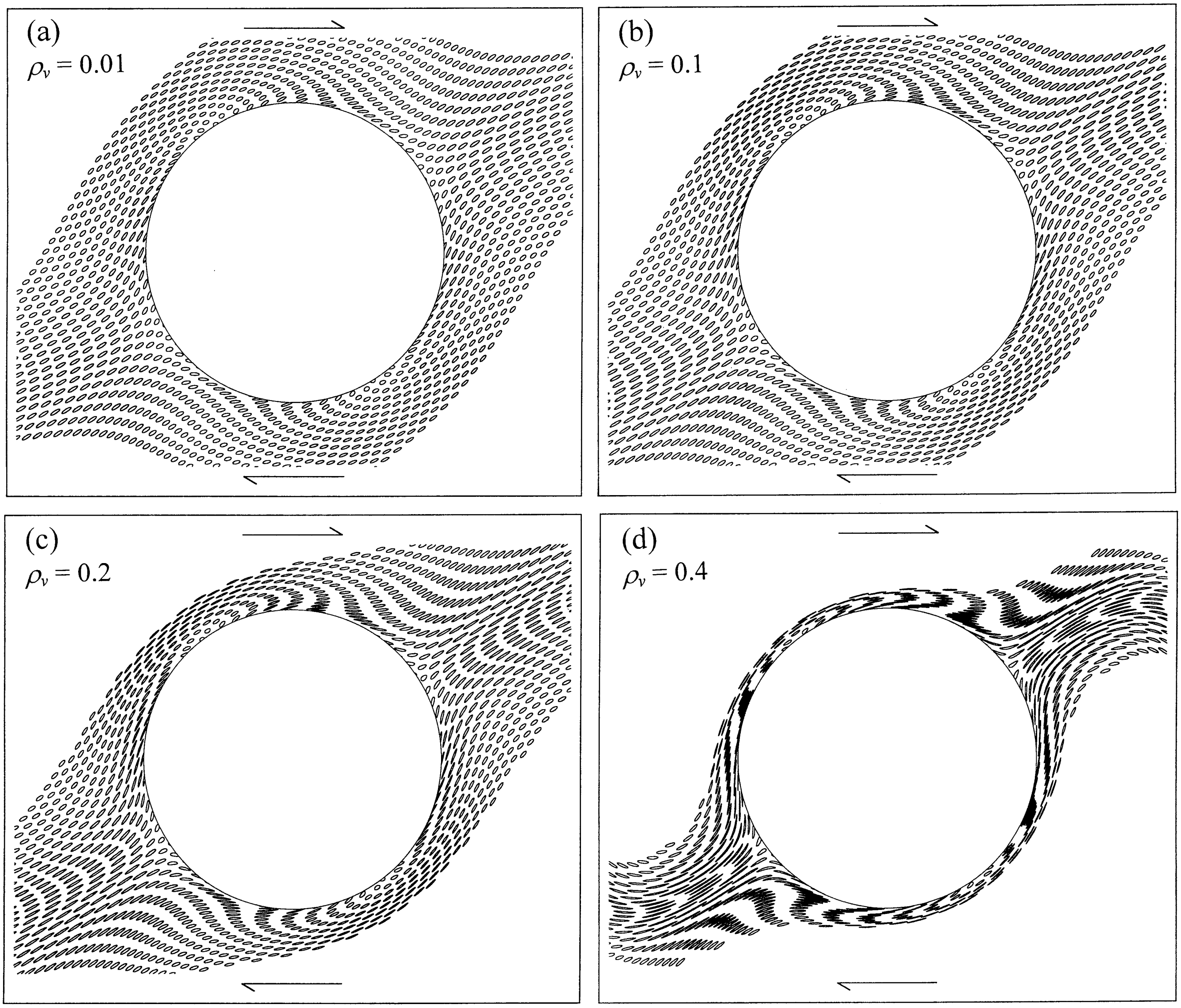

Fig. 6. Variations in the strain distributions around an inclusion for different values of ρ_v at same bulk shear ($\gamma = 1$). Note that with increase in volume concentration the finite strain around the inclusion increases. Also, note in (d) that the vergence of long axis of the strain ellipse away from the inclusion (lower part of top-right and upper part of bottom-left corners) becomes antithetic to sense of bulk shear.

mode of mantle development varies discernibly. At $\rho_v = 0.1$, the mantle at the initial stage is nearly of ϕ-type (Passchier, 1994), that turns into a typical δ-structure in the course of progressive bulk shear (Fig. 8b). When the volume concentration is large ($\rho_v = 0.2$), the mantle structure shows single ϕ-type tails on either side of the porphyroclast throughout the deformation (Fig. 8c). We performed another set of experiments at a higher size reduction rate of porphyroclast. In this case at a low volume concentration ($\rho_v = 0.01$) the mantle develops with σ-type tails, as seen in earlier physical and numerical experiments (Passchier and Simpson, 1986; Bjornerud and Zhang, 1995; Mandal et al., 2000b). With progressive increase in ρ_v the tail structures tend to be symmetrical, and attain a ϕ-type geometry (Fig. 9). In both sets of experiments, for higher values of volume concentration the tails show an overall distortion at a large finite bulk shear (Figs. 8c and 9).

5. Bulk viscosity of rocks containing rigid inclusions

Treagus (2002) has recently presented a theoretical model, based on the principles of self consistent mechanics (SCM) of composites, giving the expression of bulk viscosity of two-phase viscous mixtures as a function of phase viscosities and shape and concentration of particles or clasts. In this section we show that the theoretical analysis given in Section 3 can also be utilized to derive the bulk viscosity of suspensions containing mechanically interacting spherical rigid inclusions (cf. Mandal et al., 2000a). Gay (1968) gave a mathematical equation for measurement of

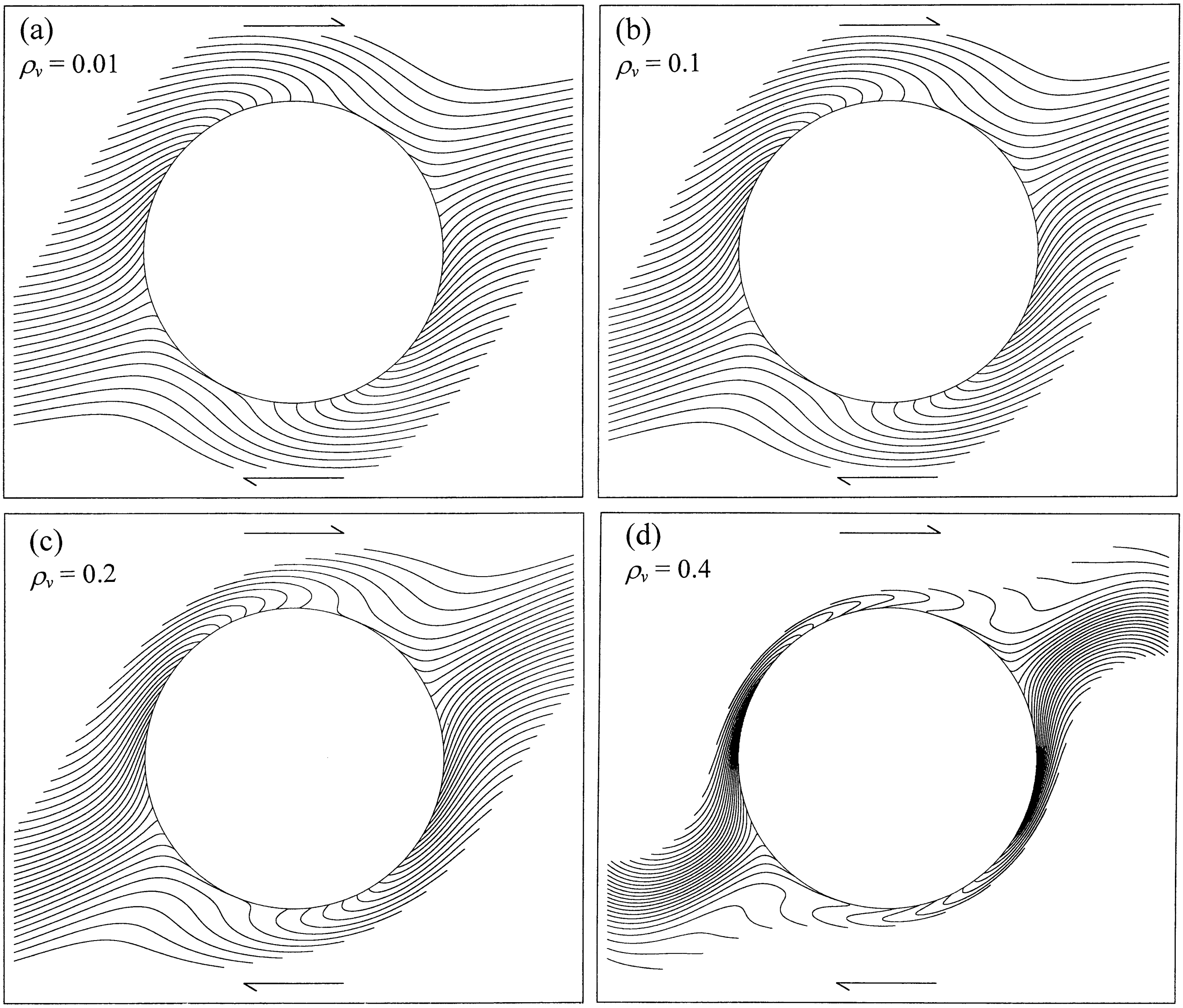

Fig. 7. Distortion patterns of passive foliations (initially parallel to the shear direction) in the neighborhood of an inclusion. Note that the distortion pattern at low values of ρ_v is exactly similar to those obtained from models based on single-inclusion system (Masuda and Ando, 1988; Mandal et al., 2001), but becomes increasingly complex at higher values of ρ_v ($\gamma = 1$).

bulk viscosity using an interaction factor, given by Happel (1957). The factor, however, has been formulated by considering only the distortion part of the bulk deformation, where the effect of mechanical coupling of rotational motion of rigid inclusions has not been taken into account. It is evident that such a coupling is likely to develop additional resistive forces in the flow and thereby modify the bulk viscosity, as outlined below.

The calculation of viscosity requires estimation of energy involved in the flow of the bulk volume under consideration (Jeffery, 1922). In our case we consider strain energies associated with distortional and rotational parts of the bulk shear, as expressed in the velocity functions in Eqs. (A2) and (A10) in Appendix A. By taking the volume integrals over the strain components in the perturbed matrix flow the energy required per unit time can be obtained from the following equation.

$$\dot{E} = V\eta\dot{\gamma}^2 + 4V\eta\int_a^b\int_0^\pi\int_o^\pi\Big[\epsilon_{rr}^2 + \epsilon_{\theta\theta}^2 + \epsilon_{\phi\phi}^2 + \tfrac{1}{2}\Big(\gamma_{r\theta}^2 + \gamma_{r\phi}^2 + \gamma_{\theta\phi}^2\Big)\Big] r^2\sin\theta \mathrm{d}r\mathrm{d}\theta\mathrm{d}\phi \quad (6)$$

The second part of Eq. (6) represents the energy associated with the perturbed flow field around rigid inclusions. Utilizing Eq. (A10), we get the strain components of the flow perturbation due to the rotational interaction, and after substituting their expressions in Eq. (6) have:

$$\dot{E}_\mathrm{R} = V\frac{3}{2}\eta\dot{\gamma}^2\left(\frac{a}{b}\right)^9\left(1 - \frac{a^3}{b^3}\right) \quad (7)$$

It is evident from Eq. (7) that the energy developing due

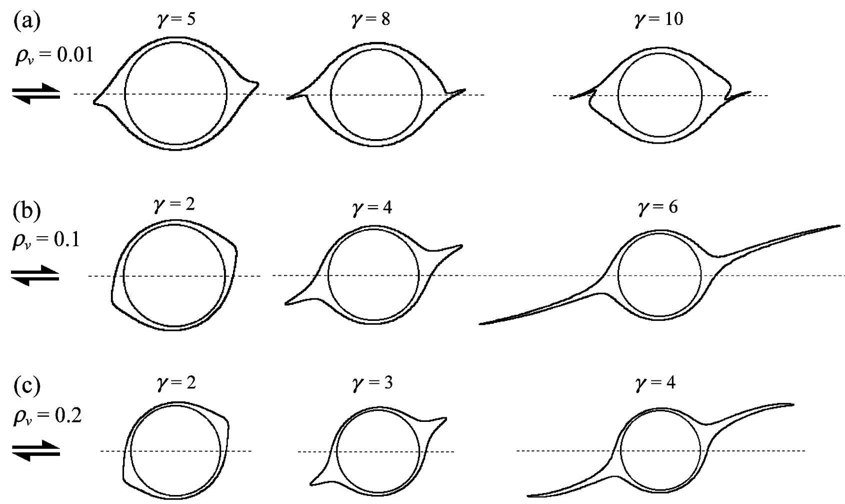

Fig. 8. Progressive development of mantle structures around porphyroclasts under varying clast concentration. The size reduction rate of porphyroclasts was kept constant at 0.125 unit/s (1 unit $= 10^{-3} \times$ initial radius of porphyroclast).

to rotational interaction tends to be zero as the inter-inclusion distance b becomes large, and will not affect the bulk viscosity of rocks containing rigid inclusions in low volume concentrations. Considering the strain components for flow perturbation due to the distortion component ϵ_{xy}, as in Eq. (A6), one can have after Happel (1957):

$$E_D = V\eta\dot{\gamma}^2 \times \left[\frac{55}{10}\frac{a^3}{b^3}\left(\frac{4(a/b)^7 + 10 - (84/11)(a/b)^2}{10(1-(a/b)^{10}) - 25(a/b)^3(1-(a/b)^4)}\right)\right] \tag{8}$$

Now, the energy required for the bulk flow is:

$$\dot{E}_b = V\eta_b\dot{\gamma}^2 \tag{9}$$

where η_b is the bulk viscosity of the rock. Balancing $\dot{E}_b$ with the total energy involved in the perturbed and unperturbed flow (Eqs. (7)–(9)), we get the expression of the bulk viscosity as:

$$\eta_b = \eta(1 + 5.5\rho_v\psi_1 + 1.5\rho_v\psi_2) \tag{10}$$

where ψ_1 and ψ_2 are interaction factors, which have the following expressions.

$$\psi_1 = \frac{4\alpha^7 + 10 - (84/11)\alpha^2}{10(1-\alpha^{10}) - 25\alpha^3(1-\alpha^4)}, \qquad \psi_2 = \alpha^6\left(1-\alpha^3\right)$$

ψ_1 and ψ_2 represent interaction factors corresponding to distortional and rotational parts of the bulk shear, respectively. In the absence of rotational interaction, i.e. $\psi_2 = 0$, the expression of bulk viscosity would be: $\eta_b = \eta(1 + 5.5\rho_v\psi_1)$, as given by Happel (1957). It may be noted that this expression of the bulk viscosity differs from the classical one: $\eta_b = \eta(1 + 2.5\rho_v)$ (Einstein, 1911; Jeffery, 1922; Taylor, 1932). This discrepancy has been discussed in detail by Happel (1957). The present study is, however, intended to show the effect of rotational interactions on the bulk viscosity of rocks undergoing rotational deformation. The analysis reveals that the bulk viscosity of inclusion-matrix systems varies non-linearly with the volume concentration parameter ρ_v (cf. Treagus, 2002), and the variation follows closely that predicted by Happel (1957). However, the rotational interaction factor ψ_2 slightly enhances the bulk viscosity (Fig. 10).

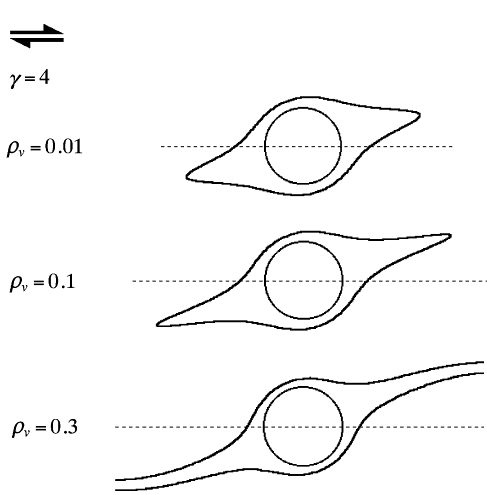

Fig. 9. Transition from σ- to ϕ-type geometry of mantle structures with increasing volume concentration. The size reduction rate of porphyroclast was 0.75 unit/s.

6. Summary and conclusions

Our analysis confirms that, in multiple-inclusion systems the volume concentration of inclusions has a significant control on the flow pattern and deformational features around individual inclusions, as revealed from physical model experiments (Ildefonse et al., 1992, 1993; Arbaret

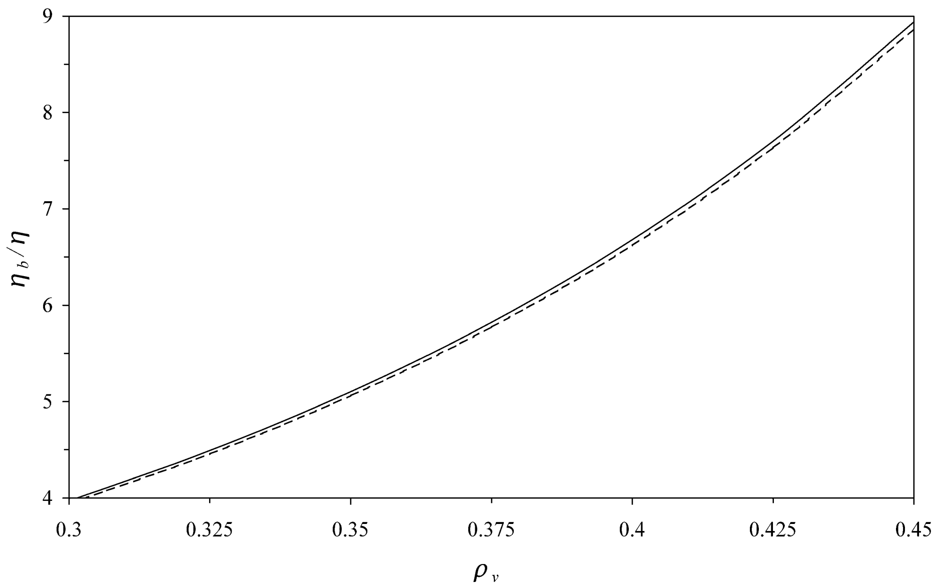

Fig. 10. Non-linear variation of bulk viscosity of rocks, normalized to matrix viscosity (η_b/η) with volume concentration parameter ρ_v ($= a^3/b^3$). The calculated plots based on the present model lie slightly above that obtained from Happel's model (dashed line).

et al., 1996). When the present model is applied to a system with low volume concentrations ($\rho_v < 0.01$), it yields results similar to those obtained from single inclusion models (e.g. Masuda and Ando, 1988; Bjornerud, 1989; Mandal et al., 2001).

The flow pattern around an inclusion in a multiple-inclusion system is characterized by an eye-shaped separatrix at low volume concentrations ($\rho_v < 0.01$), which is identical to that around a single, equant inclusion under simple shear (e.g. Mandal et al., 2001). With increase in volume concentration the effect of mechanical interactions sets in, giving rise to a pattern with a bow-tie shaped separatrix, which is phenomenologically similar to the influence of pure shear component in the general type of non-coaxial deformations (e.g. Mandal et al., 2001). In the present case, however, the stagnation points in the flow, defining the long dimension of the separatrix always lie on the central shear plane (cf. Passchier, 1994), which is not the case in single inclusion system under general deformations (Mandal et al., 2001). Separatrix of super-elliptical shape is another characteristics of interaction. The effect of mutual mechanical interaction is also evident from the overall distortion of structures, like porphyroclast tails, foliations around the inclusions (Figs. 7d and 8c), which cannot be explained by models based on single inclusion systems.

Our analysis is valid for rock systems containing equant inclusions. Earlier studies show that the flow patterns and strain distribution around inequant inclusions are much more complex (Ildefonse, 1992, 1993; Mandal et al., 2001). Again, the shape of the inclusions affects the rotation behavior, and the mechanical interactions of inequant inclusions are thus likely to be significantly different from that predicted from the present model. The other limitations of the present study are: (1) the matrix is considered as Newtonian viscous, and mechanically isotropic in the theoretical model; (2) a non-slip condition prevails at the matrix-inclusion interfaces; (3) in the multiple inclusion system the inclusions are assumed to be non-clustering, and float as isolated bodies, which, however, may cluster at large finite shear in progressive deformation (Arbaret et al., 1996) when the present theory will not be applicable; and (4) the theoretically derived rotation of interacting inclusions do not exactly match with that obtained from physical experiments, which is probably due to differences in the numerical and experimental set-ups.

The main conclusions of the present study are:

1. Lamb's (1932) hydrodynamic theory can be utilized to study the deformation of rock systems containing multiple spherical inclusions that may mechanically interact with one another.
2. The volume concentration of rigid inclusions is found to be an important physical parameter controlling the flow pattern around individual inclusions. At low volume concentrations the flow pattern around an inclusion is characterized by an eye-shaped separatrix, which is replaced by a bow-tie shaped separatrix with increase in volume concentration. At large volume concentrations the separatrix, enclosing the closed particle paths, assumes the geometry of a super-ellipse.
3. For a given bulk shear the strain distribution around a spherical rigid inclusion becomes increasingly heterogeneous with volume concentration, which conform to earlier experimental observations (Ildefonse et al., 1992).
4. For a given rate of size reduction, the mantle structures of equant porphyroclasts change with increasing volume concentration. When the size reduction rate is low, the mantle is characterized by composite δ–ϕ tails at a low

volume concentration, which becomes typical δ tails at larger volume concentration. At higher size reduction rates, σ-type tails form when the volume concentration is low. The tail structure transforms into ϕ-type with increasing volume concentration.

5. In simple shear deformation the mechanical interaction of rigid inclusions retards their rotational motion which slightly enhances the bulk viscosity of the inclusion-matrix system.

Acknowledgements

We wish to thank Drs K. Hickey and L. Arbaret for their critical comments that greatly contributed to the improvement of the paper. We also thank Dr J. Hippertt for his constructive suggestions in revising the manuscript. The present work was carried out under a project of DST, India sanctioned to NM. CC acknowledges the infrastructural facilities provided by the Indian Statistical Institute, Calcutta. SKS is grateful to CSIR, India for providing a research fellowship.

Appendix A. Derivation of velocity functions

The general expressions of the velocity components in the flow perturbations around a spherical rigid inclusion are as follows (Lamb, 1932):

$$
\begin{aligned}
u &= \frac{1}{\eta}\sum\left\{\frac{r^2}{2(2n+1)}\frac{\partial p_n}{\partial x} + \frac{nr^{2n+3}}{(n+1)(2n+1)(2n+3)}\frac{\partial}{\partial x}\frac{p_n}{r^{2n+1}}\right\} + \sum\left(\frac{\partial \Phi_n}{\partial x} + z\frac{\partial \chi_n}{\partial y} - y\frac{\partial \chi_n}{\partial z}\right)\\
v &= \frac{1}{\eta}\sum\left\{\frac{r^2}{2(2n+1)}\frac{\partial p_n}{\partial y} + \frac{nr^{2n+3}}{(n+1)(2n+1)(2n+3)}\frac{\partial}{\partial y}\frac{p_n}{r^{2n+1}}\right\} + \sum\left(\frac{\partial \Phi_n}{\partial y} + x\frac{\partial \chi_n}{\partial z} - z\frac{\partial \chi_n}{\partial x}\right)\\
w &= \frac{1}{\eta}\sum\left\{\frac{r^2}{2(2n+1)}\frac{\partial p_n}{\partial z} + \frac{nr^{2n+3}}{(n+1)(2n+1)(2n+3)}\frac{\partial}{\partial z}\frac{p_n}{r^{2n+1}}\right\} + \sum\left(\frac{\partial \Phi_n}{\partial z} + y\frac{\partial \chi_n}{\partial x} - x\frac{\partial \chi_n}{\partial y}\right)
\end{aligned}
\tag{A1}
$$

We obtain the solution of velocity components (Eq. (A1)) in two steps: one for the distortion part, and the other for the rotational part of the bulk shear flow. In obtaining the flow perturbation in response to the distortion part (ϵ_{xy}) of the bulk shear flow we follow the mathematical approach of Happel (1957). Consider a spherical coordinate system (r, θ, ϕ) with the origin at the center of the spherical inclusion under consideration (Fig. 3c), which has the relation with the Cartesian space as: $x = r\cos\theta$, $y = \mathrm{r}\cos\phi\,\sin\theta$ and $z = r\sin\phi\,\sin\theta$.

Employing the following condition: $x\zeta_x + y\zeta_y + z\zeta_z = 0$, where ζ_x, ζ_y, and ζ_z are the components of vorticity vector at a point on a spherical surface around the inclusion, Happel has given a solution of Eq. (A1) in terms of the spherical coordinates as:

$$
\begin{aligned}
v_r &= \left(6r^3A + 2rB + \frac{6}{r^2}C - \frac{3D}{r^4}\right)\dot{\gamma}\cos\phi\,\sin\theta\cos\theta\\
v_\theta &= \left(5r^3A + rB + \frac{D}{r^4}\right)\dot{\gamma}\cos\phi\,(\cos2\theta - \sin2\theta)\\
v_\phi &= \left(-5r^3A - rB - \frac{D}{r^4}\right)\dot{\gamma}\sin\phi\,\cos\theta
\end{aligned}
\tag{A2}
$$

A, B, C and D are constants and their expressions are as follows:

$$
A = -\frac{5}{2a^2}\left(\frac{\alpha^7}{10+4\alpha^7}\right)\beta,\quad B = \frac{5}{4}\left(\frac{4+10\alpha^7}{10+4\alpha^7}\right)\beta - \frac{1}{2},\quad C = -\frac{5a^3}{12}\beta,\qquad D = -\frac{5a^5}{10+4\alpha^7}\beta
\tag{A3}
$$

where

$$
\beta = \frac{10+4\alpha^7}{10(1-\alpha^{10}) - 25\alpha^3(1-\alpha^4)}
$$

and $\alpha = a/b$.

We now consider the flow perturbation that develops in response to the rotational part (ζ) of the bulk shear flow. The fluid in the shell under consideration experiences concentric motion due to the rigid rotation, following the condition: $xu + yv + zw = 0$. This is satisfied if p_n and ϕ_n in Eq. (A1) are taken to be zero. In that case:

$$
\begin{aligned}
u &= \sum z\frac{\partial \chi_n}{\partial y} - y\frac{\partial \chi_n}{\partial z};\\
v &= \sum x\frac{\partial \chi_n}{\partial z} - z\frac{\partial \chi_n}{\partial x};\\
w &= \sum y\frac{\partial \chi_n}{\partial x} - x\frac{\partial \chi_n}{\partial y}
\end{aligned}
\tag{A4}
$$

The perturbation is phenomenologically similar to that develops around a rotating rigid inclusion within a stationary fluid medium. The expression of χ_n is chosen in such a manner that the perturbation decreases with increasing distance from the surface of inclusion. Following Lamb's (1932) approach, we choose the expression of the solid harmonic function χ_n as: $\chi_{-2} = KZ/r^3$, K is a constant term, the expression of which needs to be determined by using boundary conditions. Substituting the expression of χ_n in Eq. (A4), we find:

$$u = -\frac{K}{r^3}y; \qquad v = \frac{K}{r^3}x; \qquad w = 0 \tag{A5}$$

It can be shown from Eq. (A5) that the motion develops a flow field around an inclusion rotating at an angular velocity $\dot{\gamma}/2$ in a stationary medium, the velocity components of which are:

$$v_r = 0; \qquad v_\theta = \frac{a^3}{r^3}\frac{\dot{\gamma}}{2}r\cos\phi; \qquad v_\phi = -\frac{a^3}{r^3}\frac{\dot{\gamma}}{2}r\cos\theta\sin\phi \tag{A6}$$

We are now in a position to determine the angular velocity of mechanically interacting spherical inclusions, utilizing the mathematical functions in Eq. (A6). Consider the spherical volume as in Fig. 3a. In the absence of any mechanical interaction the velocity components in the fluid at the surface of the shell ($r = b$) due to rotational component ζ in terms of the spherical co-ordinates are:

$$v_r^o = 0; \qquad v_\theta^o = \frac{\dot{\gamma}}{2}b\cos\phi; \qquad v_\phi^o = -\frac{\dot{\gamma}}{2}b\sin\phi\cos\theta \tag{A7}$$

The tangential velocity component in Eq. (A7) acts oppositely to retard the body rotation of the fluid shell. From Eqs. (A6) and (A7), we can then write:

$$\omega' b\cos\phi = \frac{\dot{\gamma}}{2}b\cos\phi - \frac{a^3}{b^3}\frac{\dot{\gamma}}{2}b\cos\phi \tag{A8}$$

where ω' is the effective rate of rotation of the inclusion at the center of the shell.

The equation finally takes a simple form:

$$\omega' = \left(1 - \frac{a^3}{b^3}\right)\frac{\dot{\gamma}}{2} \tag{A9}$$

Eq. (A9) shows that the inclusion rotates at a slower rate than single inclusions rotating at a rate of $\dot{\gamma}/2$. The perturbation due to rotational interaction can be considered as the velocity differences in the matrix developing due to the difference in the rotation rate. It then follows from Eq. (A5):

$$v_{r\mathrm{R}} = 0; \qquad v_{\theta\mathrm{R}} = \frac{\dot{\gamma}}{2}\frac{a^6}{b^3 r^2}\cos\phi;$$
$$v_{\phi\mathrm{R}} = -\frac{\dot{\gamma}}{2}\frac{a^6}{b^3 r^2}\cos\theta\sin\phi \tag{A10}$$

References

Arbaret, L., Diot, H., Bouchez, J.-L., 1996. Shape fabrics of particles in low concentration suspensions: 2D analogue experiments and application to tiling in magma. Journal of Structural Geology 18, 941–950.

Bell, T.H., 1985. Deformation partitioning and porphyroblast rotation in metamorphic rocks: a radical reinterpretation. Journal of Metamorphic Geology 3, 109–118.

Bjornerud, M.G., 1989. Mathematical model for folding of layering near rigid inclusions in shear deformation. Journal of Structural Geology 11, 245–254.

Bjornerud, M.G., Zhang, H., 1995. Flow mixing inclusion matrix coherent mantle growth and the development of porphyroclast tails. Journal of Structural Geology 17, 1347–1350.

Einstein, A., 1911. Eine neue Bestimmung der Molekuldimensionen. Annual D. Physik 34, 591.

Ferguson, C.C., 1979. Rotations of elongate rigid particles in slow non-Newtonian flows. Tectonophysics 60, 247–262.

Fernandez, A., 1987. Preferred orientation developed by rigid markers in two-dimensional simple shear strain: a theoretical and experimental study. Tectonophysics 136, 151–158.

Freeman, B., 1985. The motion of rigid ellipsoidal particles in slow flows. Tectonophysics 113, 163–183.

Gay, N.C., 1968. Pure shear and simple shear deformation of inhomogeneous viscous fluids. 1. Theory. Tectonophysics 5, 211–234.

Ghosh, S.K., 1975. Distortion of planar structures around rigid spherical bodies. Tectonophysics 28, 185–208.

Ghosh, S.K., Ramberg, H., 1976. Reorientation of inclusions by combination of pure shear and simple shear. Tectonophysics 34, 1–70.

Happel, J., 1957. Viscosity of suspensions of uniform spheres. Journal of Applied Physics 28, 1288–1292.

Hickey, K.A., Bell, T.H., 1999. Behaviour of rigid objects during deformation and metamorphism; a test using schists from the Bolton Syncline, Connecticut, USA. Journal of Metamorphic Geology 17, 210–228.

Ildefonse, B., Sokoutis, D., Mancktelow, N.S., 1992. Mechanical interactions between rigid particles in a deforming ductile matrix. Analogue experiments in simple shear flow. Journal of Structural Geology 14, 1253–1266.

Ildefonse, B., Launeau, P., Bouchez, J.-L., Fernandez, A., 1993. Effect of mechanical interactions on the development of shape preferred orientations: a two-dimensional experimental approach. Journal of Structural Geology 14, 73–83.

Jeffery, G.B., 1922. The motion of ellipsoidal particles immersed in a viscous fluid. Proceedings of Royal Society of London A 120, 161–179.

Jezek, J., Schulmann, K., Segeth, K., 1996. Fabric evolution of rigid inclusions during mixed coaxial and simple shear flows. Tectonophysics 257, 203–221.

Jezek, J., Saic, S., Segeth, K., Schulmann, K., 1999. Three-dimensional hydrodynamical modeling of viscous flow around a rotating ellipsoidal inclusion. Computers & Geosciences 25, 547–558.

Johnson, S.E., 1993. Testing models for the development of spiral-shaped inclusion trails in garnet porphyroblasts: to rotate or not to rotate, that is the question. Journal of Metamorphic Geology 11, 635–659.

Lamb, H., 1932. Hydrodynamics. Cambridge University Press, Cambridge.

Lisle, R.J., 1988. The superellipsoidal form of coarse clastic sediment particles. Mathematical Geology 20, 879–890.

Mandal, N., Chakraborty, C., Samanta, S.K., 2000a. An analysis of anisotropy of rocks containing shape fabrics of rigid inclusions. Journal of Structural Geology 22, 831–839.

Mandal, N., Samanta, S.K., Chakraborty, C., 2000b. Progressive development of mantle structures around elongate porphyroclasts: insights from numerical models. Journal of Structural Geology 22, 993–1008.

Mandal, N., Samanta, S.K., Chakraborty, C., 2001. Numerical modeling of heterogeneous flow fields around rigid objects with special reference to particle paths, strain shadows and foliation drag. Tectonophysics 330, 177–194.

Masuda, T., Ando, S., 1988. Viscous flow around a rigid spherical body: a hydrodynamical approach. Tectonophysics 148, 337–346.

Masuda, T., Mizuno, N., 1996. Computer modeling of mantled porphyroclasts in Newtonian and non-Newtonian simple shear viscous flows. Journal of Structural Geology 18, 1487–1491.

Masuda, T., Michibayashi, K., Ohata, H., 1995. Shape preferred orientation of rigid particles in a viscous matrix: reevaluation to determine parameters of ductile deformation. Journal of Structural Geology 17, 115–129.

Passchier, C.W., 1987. Stable positions of rigid inclusions in non-coaxial flow: a study in vorticity analysis. Journal of Structural Geology 9, 679–690.

Passchier, C.W., 1994. Mixing in flow perturbations: a model for development of mantle porphyroclasts in mylonites. Journal of Structural Geology 16, 733–736.

Passchier, C.W., Simpson, C., 1986. Porphyroclast systems as kinematic indicators. Journal of Structural Geology 8, 831–844.

Pennacchioni, G.P., Fasolo, L., Cecchi, M.M., Salasnich, L., 2000. Finite-element modeling of simple shear flow in Newtonian and non-Newtonian fluids around circular rigid particle. Journal of Structural Geology 22, 683–692.

Reed, L.J., Tryggvason, E., 1974. Preferred orientation of rigid particles in a viscous matrix deformed by pure shear and simple shear strain. Tectonophysics 24, 85–98.

Samanta, S.K., Mandal, N., Chakraborty, C., 2002. Development of structures under the influence of heterogeneous flow field around rigid inclusions: insights from theoretical and numerical models. Earth Science Reviews in press.

Stallard, A.R., Hickey, K.H., 2001. Shear zone vs. folding origin for spiral inclusions in the Canton Schist. Journal of Structural Geology 23, 1865–1881.

Stewart, L.K., 1997. Experimental investigation of the effects of fluid heterogeneity upon the motion of rigid ellipsoidal inclusions during bulk inhomogeneous shortening. Journal of Structural Geology 19, 1231–1243.

Taylor, G.I., 1932. The viscosity of a fluid containing small drops of another fluid. Proceeding of Royal Society of London A 138, 41–48.

ten Brink, C., Passchier, C.W., 1995. Modeling of mantled porphyroclasts using non-Newtonian rock analogue materials. Journal of Structural Geology 17, 131–146.

Tikoff, B., Teyssier, C., 1994. Strain and fabric analyses based on porphyroclast interaction. Journal of Structural Geology 16, 691–704.

Treagus, S.H., 2002. Modelling the bulk viscosity of two-phase mixtures in terms of clast shape. Journal of Structural Geology 24, 57–76.